Graphene on the Ir(111) surface: from van der Waals to strong bonding

2010 New J. Phys. 12 113016

(http://iopscience.iop.org/1367-2630/12/11/113016)

New Journal of Physics
The open-access journal for physics

Graphene on the Ir(111) surface: from van der Waals to strong bonding

R Brako[1,3], D Šokčević[1], P Lazić[1,2,4] and N Atodiresei[2]

[1] Ruđer Bošković Institute, 10000 Zagreb, Croatia
[2] Institut für Festkörperforschung and Institute for Advanced Simulation, Forschungszentrum Jülich and JARA, 52425 Jülich, Germany
E-mail: radovan@thphys.irb.hr

New Journal of Physics **12** (2010) 113016 (17pp)
Received 1 July 2010
Published 10 November 2010
Online at http://www.njp.org/
doi:10.1088/1367-2630/12/11/113016

Abstract. We calculated the properties of a graphene monolayer on the Ir(111) surface, using the model in which the periodicities of the two structures are assumed equal, instead of the observed slight mismatch which leads to a large superperiodic unit cell. We used the density functional theory approach supplemented with the recently developed van der Waals-density function (vdW-DF) non-local correlation functional. The latter is essential for treating the vdW interaction, which is crucial for the adsorption distances and energies of the rather weakly bound graphene. When additional iridium atoms are put on top of graphene, the electronic structure of C atoms acquires the sp^3 character and strong bonds with the iridium atoms are formed. We discuss the validity of the approximations used and their relevance to other graphene–metal systems.

[3] Author to whom any correspondence should be addressed.
[4] Present address: Department of Materials Science and Engineering, Massachusetts Institute of Technology, Cambridge, MA 02139, USA.

Contents

1. Introduction

Graphene is a one-atom-thick two-dimensional structure of carbon atoms arranged in a honeycomb lattice. It is (conceptually at least) at the origin of all other graphitic forms [1], including three-dimensional graphite, one-dimensional carbon nanotubes and zero-dimensional fullerenes. The planar geometry and the exceptional strength of graphene [2] are due to the sp^2 bonds between atoms. Single-layer graphene has been obtained by micromechanical cleavage of graphite and by growth on SiC and metal surfaces. The recent increased interest in graphene is due both to the theoretical implications of its unique electronic properties and to its potential applicability, in particular as a novel material for electronics.

As the building block of graphite and as the adsorbate on many surfaces, graphene bonds to its surroundings only weakly, and the character of the bonding is largely van der Waals (vdW). Occasionally, stronger bonding occurs without destroying the geometry of the graphene lattice [3], for example on Ni(111) [4] and Ru(0001) [5]–[7] surfaces. Graphene on Ir(111) is an example where, depending on the conditions, both kinds of bonding can occur. Monolayer graphene is vdW physisorbed, and the characteristic graphene lattice can be clearly seen in scanning tunneling microscope (STM) images [8], whereas with additional Ir clusters on top, the carbon–metal bonds become stronger.

Large-cell density functional theory (DFT) calculations of graphene on Ir(111) have been performed using the Perdew–Burke–Ernzerhof generalized gradient approximation (PBE GGA) [8] and local density approximation (LDA) [9]. However, experiments and calculations reveal a subtle interplay between vdW bonding and stronger electronic interaction with the substrate. The vdW interaction is not properly described in the standard local (LDA) and semilocal (GGA) DFT functionals, which poses a serious obstacle to the complete understanding of the nature of the bonding.

In this paper, we apply the recently developed extension to the DFT, which replaces the semilocal (i.e. depending upon the gradient of the electronic density) correlation term with a fully non-local one (depending upon the electronic densities at different points in space), which can describe the vdW forces even between two fragments of matter with non-overlapping electronic densities. Due to computational complexity we had to abandon the large

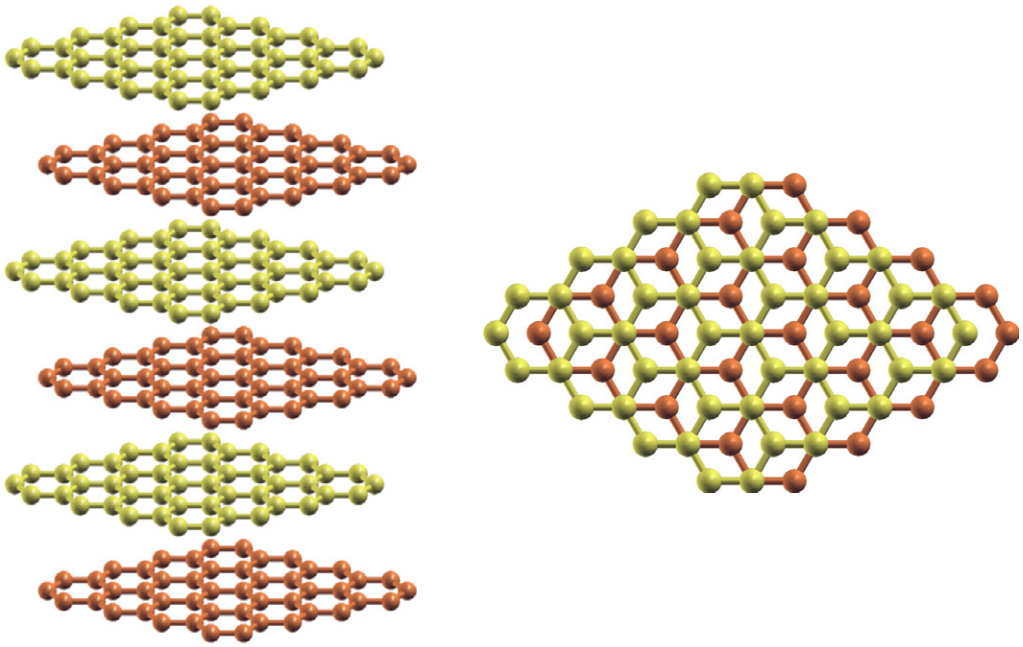

Figure 1. Structure of graphite (side and top views). The layers are stacked in AB order, so that half of the C atoms lie in chains along the direction perpendicular to the graphene planes, while the other half alternate in the other two high-symmetry positions. The periodicity in the perpendicular direction is c, i.e. the interlayer distance is $c/2$. For clarity, c has been exaggerated by about a factor of 3.

supercell, which aims to describe more realistically the graphene and Ir(111) surface with their slightly different atomic periodicities, and opt for an approximate description by a smaller commensurate unit cell. While the quantitative accuracy of the results suffers (but we argue that it is quite a limited and controlled problem), the approximation makes the transition from weak to strong bonding easier to analyse and understand.

2. Graphene binding in graphite

We first applied our methods to graphite, i.e. graphene sheets arranged in the most stable AB stacking, shown in figure 1. This is a much studied system with good experimental data and calculated values of structural and energetic parameters. It has the same complexities of having both weak vdW and strong in-plane chemical bonds as the main topic of our interest, graphene on Ir(111). A single sheet of graphene presents no difficulties for the standard DFT GGA approach, giving the C–C distance of 1.42 Å, corresponding to a lattice constant of 2.46 Å, in agreement with the experiment. Next, we performed the density functional calculations of stacks of graphene sheets using several flavours of LDA and GGA, implemented in several numerical codes. The size and shape of the unit cell, the number of k-points and other parameters were adapted to the particular DFT program used, taking care that full convergence is obtained. Thus, the value of the energy cutoff for the calculation in abinit program was 50 Hartree, more than twice as large as the corresponding parameter for dacapo code, which uses ultrasoft

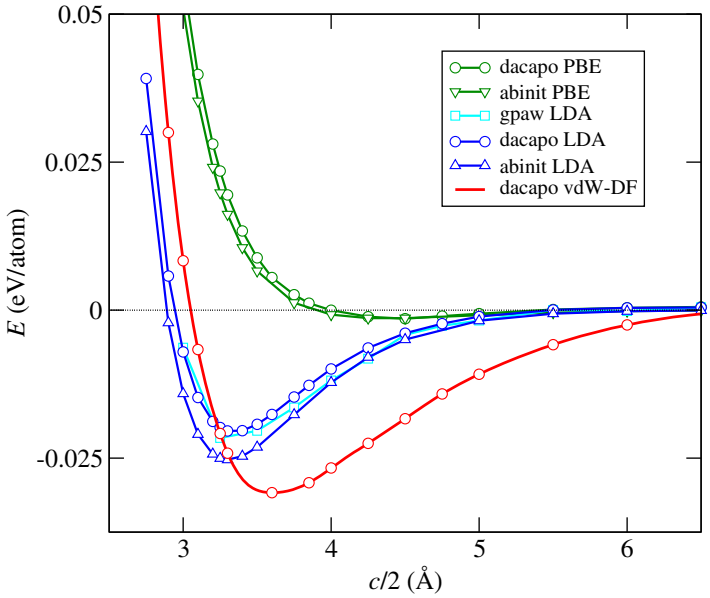

Figure 2. Binding energies of graphite AB structure as a function of interlayer distance: comparison of various DFT codes, plane-wave-based dacapo (https://wiki.fysik.dtu.dk/dacapo/), abinit (the ABINIT code is a collaborative project of the Université Catholique de Louvain, Corning, Inc., and other collaborators; http://www.abinit.org) [10], and real-space gpaw [11] (https://wiki.fysik.dtu.dk/gpaw/). Local LDA and semilocal PBE GGA results are shown. The curve labelled vdW-DF is the energy when the PBE GGA correlation has been replaced by a fully non-local vdW-DF correlation [12] using the JuNoLo numerical code [13] (http://www.fz-juelich.de/iff/src/th1/JuNoLo/).

pseudopotentials and is less demanding in that respect. The calculated cohesive energies are shown in figure 2 as a function of the interlayer separation. After that, we used the non-local vdW-DF functional for the correlation [12].[5]

The pure DFT results agree well for all the programs used, and are even quite insensitive to the (lack of) full self-consistency. For example, dacapo calculations use the PW91 GGA functional. Nevertheless, the dacapo LDA curve shown in the figure, obtained by evaluating the LDA functional on the electron density calculated with PW91, agrees quite well with the fully self-consistent abinit LDA results. GGA calculations give little or no bonding, and LDA gives (apparently) reasonable bonding energies and distances, comparable to experimental values. The reason for the failure of GGA is intuitively clear: the semilocal gradient approximation cannot describe well the inherently non-local vdW interaction, which exists even between subsystems with completely non-overlapping electronic densities. The apparent success of LDA is somewhat perplexing, since it is even more local than the more advanced GGA, the latter indeed being more successful when it comes to chemically bound systems. There are strong indications that the agreement of the LDA results is largely fortuitous, as discussed further on.

We have further investigated the problem by applying the vdW-DF theory [12], which is at present the most promising approach for treating the non-local correlation. It consists in

[5] For a review of the method used by the authors for vdW-DF, see [14].

replacing the semilocal (gradient) part of the GGA correlation functional by a fully non-local term, which still depends only upon the electronic density, in the true spirit of the DFT. We have applied vdW-DF as implemented in JuNoLo code [13] in a post-processing approach, i.e. we used the electron densities obtained in the standard GGA calculation to evaluate the non-local vdW-DF correlation and inserted it into the total energy instead of the semilocal correlation. This approach is, of course, not fully self-consistent, since the DFT potential and the Kohn–Sham wavefunctions, and hence the electron density can depend on the details of the correlation functional used. However, a recent self-consistent implementation of the vdW-DF correlation functional shows that the differences are negligible [15]. We have therefore relied on the post-processing approach that is less time consuming and avoids any intervention in the code of the DFT programs. Changing the correlation contribution changes the total energy and therefore the forces acting on the atoms as well. However, all atomic configurations that we consider here have high symmetry, where we can sweep the interesting range of interlayer separation 'by hand' in order to find the optimum configuration. The lack of fully self-consistent atomic relaxations inherent to such an approach is not a major problem, as discussed later on. We furthermore note that we have not followed the suggestion put forward by the authors of the vdW-DF theory to use the revPBE exchange functional [12], and have instead continued using the PBE exchange. Although revPBE exchange seems to compensate for too large binding energies for several vdW bound systems, it gives worse equilibrium distances, and the same improvement does not seem to occur in cases of strong bonding.

The vdW-DF results shown by a thick line in figure 2 are qualitatively similar to the LDA results, but with some important differences. The vdW-DF attractive potential has clearly a longer range than LDA, which reflects the long-range nature of the vdW attraction and reveals the fortuitous character of the agreement with LDA around the minimum. To our knowledge, the most complete *ab initio* treatment of graphite is the quantum Monte Carlo calculation in [16], where an overview of earlier theoretical and experimental results is also given. The authors note that local or semilocal approximations to DFT do not correctly describe the long-range correlation, owing to the local character of the exchange and correlation functionals. They get the interlayer distance of 3.43 Å, while the experimental value is 3.35 Å. We obtain 3.3 Å using LDA DFT and 3.6 Å using the non-local vdW-DF correlation, both in agreement with other similar calculations quoted in [16]. The binding energy is not useful for comparison because there are no good experimental data. Thus, although the vdW-DF interlayer spacing agrees with experiment less well than the LDA value, the long-range attractive tail of the vdW potential is well reproduced, while it is almost missing in LDA.

Recently, it was found that the behavior of the non-retarded vdW interaction between non-overlapping anisotropic nanostructures that have a zero electronic energy gap should be different from that predicted from the usual sum of R^{-6} contributions [17], but probably this is relevant only in the extreme asymptotic regime.

We conclude that the inclusion of the vdW interaction is essential for reproducing the physical properties of graphite and that the vdW-DF approach successfully treats all aspects of the graphene binding in graphite.

3. Structure of graphene on Ir (111) surface

Graphene monolayers of high structural quality, extending over tens of nanometres and even up to micrometre size, orientationally well aligned with the substrate, have recently been obtained

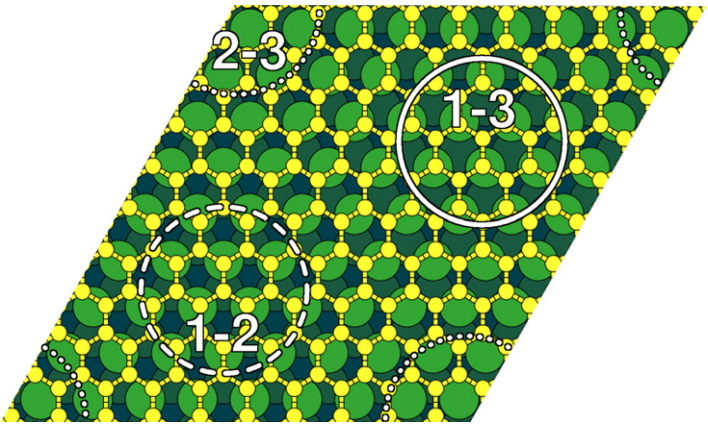

Figure 3. Moiré superstructure of 10×10 graphene on a 9×9 Ir(111) unit cell. The C atoms are (approximately) above the first and third layer Ir atoms within the circle labelled 1–3, above the first and second layers in 1–2 and above the second and third layers in 2–3. The regions that we denote by 1–3, 1–2 and 2–3 are called 'hcp', 'fcc', and 'atop' regions in [8] and [9], according to the Ir(111) high-symmetry site that is surrounded by C-atom rings, i.e. which is *not* covered by a graphene atom.

by hydrocarbon decomposition on Ir(111) [8]. The lattice constants of graphene and the Ir(111) surface differ at room temperature by about 10%, and the STM micrographs clearly show the moiré pattern due to the lattice mismatch. In figure 3, the supercell with a 10×10 graphene lattice on top of a 9×9 structure of iridium atoms is shown. A further intriguing feature is observed when additional iridium atoms are adsorbed on top of the graphene. STM images show that the adatoms form regular arrays on clusters, selectively bound to certain regions of the moiré pattern [8, 9].

Density functional calculations have been performed employing the PBE GGA functional [8] and LDA functional [9] on a supercell similar to the one in figure 3. It was found that the PBE GGA functional gives almost no bonding of graphene monolayer on Ir(111) ([8] erratum, [18]), while the LDA functional gives reasonable results for bonding energies and interatomic distances, both without and with additional clusters on top [9]. These results are qualitatively reminiscent of our results for graphite, i.e. we again see the apparent success of the quite basic LDA in comparison with GGA, which indicates that a more detailed investigation is necessary.

Our strategy is similar to the approach used for graphite in section 2. We start with the standard DFT and later investigate the effects of the nonlocal correlation. The GGA and LDA calculations in [8, 9] using the realistic large unit cell shown in figure 3 require a very large amount of computational resources, and similar calculations with the non-local correlation included via JuNoLo code [13] are at present beyond computational capabilities. We instead adopt the approach of using a small (1×1) unit cell obtained by compressing the Ir(111) substrate in the surface plane (coordinates x, y) so that it matches the lattice constant of graphene. By changing the phase of the carbon atoms with respect to the underlying lattice of Ir atoms, we are able to simulate (approximately) any point in the supercell in figure 3. The much smaller size of the problem makes it possible to also check carefully the convergence of

the calculation with respect to parameters such as the energy cutoff, the number of k-points, the thickness of the vacuum layer separating the periodic repeating slabs in the z-direction, etc. Of course, some quantitative accuracy of the calculations is sacrificed in this approach. We have performed the most calculations for the region labelled 1–3, which both experiment and calculations show to be most strongly bonding, with only a few checks of the other regions.

Calculations of commensurate graphene–metal surface systems have been performed for several metal surfaces, by adjusting either the substrate lattice constant [19] or the graphene lattice constant [20]. We shall discuss these calculations in more detail later on.

The mismatch of the lattice constant of graphene (2.46 Å) and that of the Ir(111) surface (2.73 Å, corresponding to the conventional fcc lattice constant $a_0 = 3.86$ Å) is about 10%, clearly larger than those in [19], which are in the range of 0.8–3.8%. In order to minimize possible artefacts due to the squeezing of the iridium substrate to fit the graphene lattice, we optimized the lattice constant of the iridium substrate in the z-direction. To that end, we performed calculations of iridium bulk with compressed (111) planes and allowed it to relax in the perpendicular direction. The lattice constant in the z-direction increased by about 10% to 4.24 Å, and we used this lower-symmetry iridium lattice, compressed in the x–y directions and expanded in z, as the substrate in our calculations. From the point of view of quantitative accuracy, a calculation using a large supercell and 'natural' iridium substrate would be preferred, but our approach enables a clear insight into the bonding properties, which would be at risk of remaining buried and hard to see in the more realistic large calculation.

Another important aspect of graphene interaction with the Ir(111) surface can be inferred from the band structure of Ir(111) along high-symmetry directions of the surface Brillouin zone. Our calculations based on the DFT Kohn–Sham eigenstates [21] as well as angle-resolved photoemission spectroscopy (ARPES) experiments [21, 22] show that there is an energy gap around the K-point of the surface Brillouin zone, extending from just below the Fermi level down to almost 1.5 eV binding energy. The vertex of the 'Dirac cone' of the π-bands of graphene adsorbed on Ir(111) lies entirely within this gap [22]. The weak interaction of graphene with the iridium substrate can be attributed to this mismatch of the electronic states, since the unsaturated π-bands of the Dirac cones do not have any substrate states with the same momentum k and energy E to hybridize with. We have also checked the band structure of our compressed iridium surface and found that the band gap around the K-point is still present and has a similar shape, which implies that the weak character of the graphene interaction with Ir(111) will not be much affected by the use of the compressed substrate.

In our DFT calculations, we use a three-layer Ir(111) slab with the adjusted lattice constants in the x–y and the z-directions as explained above. It would have been easy to use a thicker substrate, but this would add no further quantitative accuracy, considering other simplifications and approximations used. The vacuum layer separating the periodically repeating structures in the z-direction was about 18 Å. We used dacapo program. The energy cutoff was 440 eV and there were 54 k-points in the x–y plane.

4. Density functional theory (DFT) calculations of graphene on Ir(111) and Ir–graphene–Ir sandwiches

For our calculations, we have chosen four characteristic structures of graphene on iridium, shown in figure 4. The structures are periodic in the x–y plane and extend to infinity, but for clarity we show only a small symmetric cluster of atoms for each one. There are two atoms

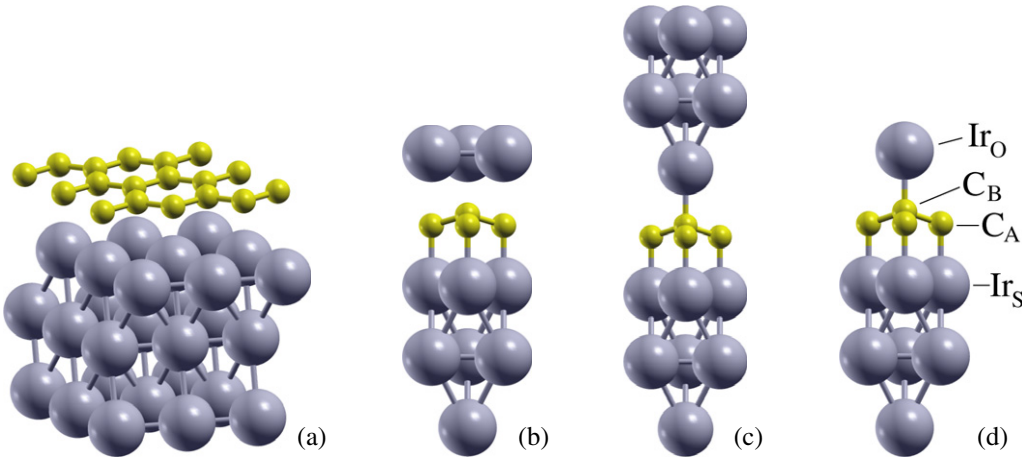

Figure 4. The four structures considered in the paper. For clarity, only a few atoms from each atomic layer are shown in structures (b)–(d).

in the unit cell of graphene, which in the following we denote by C_A and C_B, as illustrated in figure 4(d). We denote the iridium atoms in the first substrate layer by Ir_S and the atoms in the first overlayer as Ir_O.[6]

The structures were chosen so that they illustrate Ir–C bonds of various character, with the overall bonding strength increasing from structure (a) to structure (d). The iridium substrate is modelled by three atomic layers in all cases. The structures are: (a) monolayer graphene on Ir(111) with C_A above Ir_S and C_B above the third layer Ir, which illustrates the most stable regions of the moiré pattern of monolayer graphene on Ir(111). (b) Graphene monolayer as in (a), but with a single overlayer of iridium atoms, with Ir_O located above the centres of the hexagonal rings of the graphene. (c) Three additional layers of iridium, with Ir_O above C_B. (d) A single Ir overlayer, with atoms in the same positions as in the first layer in (c). In (c) and (d), there is one iridium atom below C_A and another one above C_B, which models the geometries of the stable iridium clusters on top of graphene observed in the experiment.

4.1. Standard DFT only

We first calculated the dependence of the interaction energy upon Ir–graphene separation for structures (a)–(d), using the standard LDA and GGA PBE functionals. The results are shown in figure 5. Two comments are in order. For structure (a), the energy scale in figure 5 is smaller by a factor of two, since the graphene has iridium atoms only on one side, and the interaction (in particular, the repulsion at small distances) is expected to scale with the number of neighbouring atomic planes. Secondly, for the sandwich structures (b)–(d) the graphene layer was at the beginning of the calculations placed symmetrically between the nearest Ir layers, each of them at a distance of z_{Ir-g}, but was allowed to relax in the course of the calculation. At small separations z_{Ir-g} the graphene buckles, with C_A atom moving towards Ir_S and C_B towards the overlayer. This is not a major problem, since the two atoms move by almost the same amount in the opposite direction, even in the case of the less symmetrical structure (b), so that z_{Ir-g} still measures the

[6] The labels A and B for the two inequivalent sublattices of graphene should not be confused with the same letters used to denote the graphene stacking in section 2. Both notations are widely used.

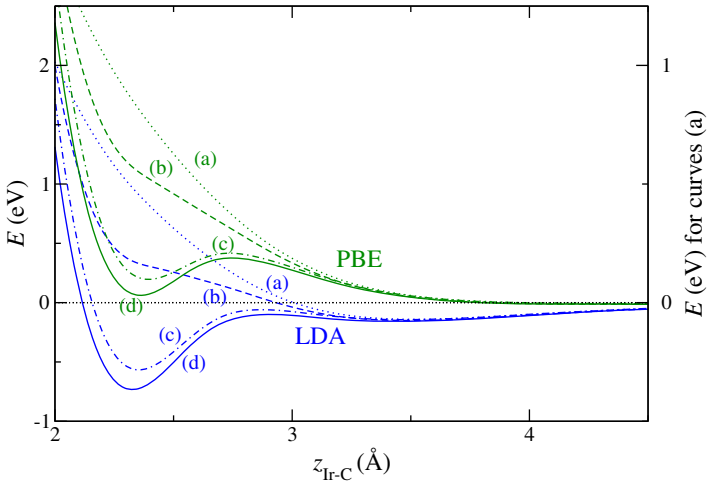

Figure 5. DFT (LDA and PBE GGA) energies for graphene on Ir, structure (a) in figure 4, and Ir–graphene–Ir sandwiches, structures (b)–(d) in figure 4. In this and the following graphs the energies are given per unit cell, i.e. two C atoms and one Ir atom in each iridium layer.

z-averaged position of the graphene plane. There is no buckling at $z_{\mathrm{Ir-g}}$ separations larger than say 3 Å. Since the relaxation was done according to the forces calculated in GGA functional, which does not develop any appreciable attractive potential well at these distances, there was no danger that the graphene layer would be attracted to the iridium atoms on one side. Iridium atoms were not relaxed.

At distances $z_{\mathrm{Ir-g}}$ larger than 3.3 Å all LDA curves in figure 5 are almost identical to one another, as are all GGA curves between themselves, i.e. there is little dependence of the interaction energy on where exactly the graphene C atoms lie above the substrate Ir atoms, and where the additional Ir atoms in structures (b)–(d) lie above graphene atoms. At small graphene–Ir distances the sandwich structures (b)–(d) show the tendency to form a strong bond between graphene and iridium atoms, with energy minimum around 2.3 Å. Unlike the large-$z_{\mathrm{Ir-g}}$ case, the strength of the graphene–iridium bonding is quite sensitive to the relative positions of the atoms. Thus, in the unfavourable structure (b), where the Ir atoms in the additional layer do not lie directly above the C atoms, there is only a kink in the interaction energy at about 2.3 Å, hinting that there is a tendency towards strong chemical bonding. The structures (c) and (d) develop a distinct potential well around that distance, which is not deep enough in the PBE GGA functional calculation, but with the LDA functional it becomes the stable configuration with more than 0.5 eV binding energy. Note that the quantity $z_{\mathrm{Ir-g}}$ measures the distance to the average z-coordinate of the graphene layer, and since there is a buckling of about 0.2 Å of C atoms towards the nearest Ir atom, the Ir–C distance is actually around 2.1 Å, as discussed in more detail later on.

These results prompt us to re-evaluate even the standard DFT calculations in the region of strong bonding at small Ir–C distances, where the graphene layer significantly changes its electronic character. Until now we have consistently used the lattice constant of free graphene, assuming that it is optimal for the bound system too (and we went to the trouble of compressing the Ir layers accordingly). This may not be true in the region of strong bonding, and we first check this.

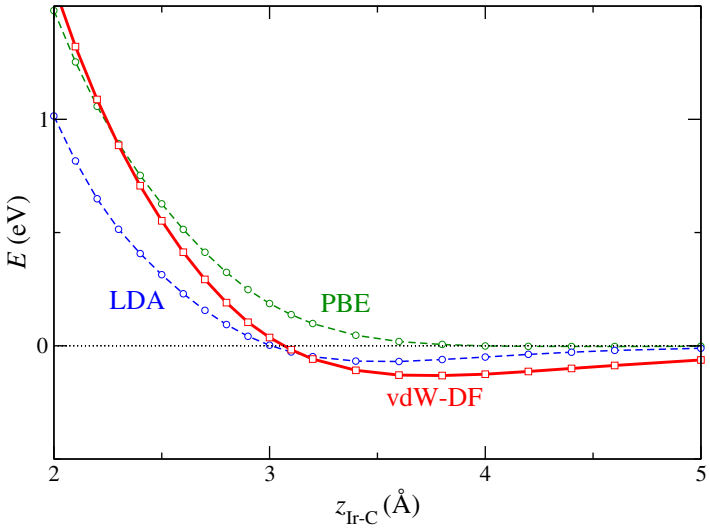

Figure 6. Standard DFT (LDA and PBE GGA) and vdW-DF energies for a graphene monolayer on Ir(111), structure (a) in figure 4.

To that end, we performed standard DFT calculations of structures (c) and (d) with the lattice constant in the x–y plane slightly expanded from the value of free graphene (3.478 Å, C–C distance 1.42 Å) and accordingly reduced Ir layer spacing in the z-direction, and checked whether there was any improvement of the total energy. In order to evaluate the bonding energy we also had to calculate the energy of separated Ir and graphene slabs (corresponding to $z_{\text{Ir–g}} \to \infty$) for the expanded lattice constant, and subtract it from the energy of the interacting system. We have repeated this procedure for several values of the expansion, in order to find the value that gives minimum total energy. In figure 7, we show the results for structures (c) and (d). The unconnected circles are the non-optimized results (i.e. $a_0 = 3.478$ Å) for the two structures taken from figure 5, while the connected circles are the best results obtained by expanding the lattice as explained above. We see that the energy improves significantly in the region of strong bonding, where the optimum lattice constant at the position of the minimum, $z_{\text{Ir–g}} \sim 2.3$ Å, increases from the free graphene value of 3.478 Å to 3.65 Å for structure (c) and to 3.72 Å for structure (d). The fact that in the region of weak binding, for $z_{\text{Ir–g}} > 3$ Å, there is no improvement of energy and the optimal lattice constant remains at the value of free graphene (i.e. the large graphene stiffness dominates the energy balance) indicates that the procedure of optimizing the lattice constant is consistent with other approximations used in the calculations.

4.2. DFT with vdW-DF

The standard DFT results shown in figure 5 reveal interesting details about the transition to strong bonding at small $z_{\text{Ir–g}}$, but still lack the vdW interaction at intermediate and large separations. In order to account for the effects of the long-range correlation, we applied the vdW-DF approach in a post-GGA procedure to DFT results for structures (a), (c) and (d). Here the full power of the vdW-DF correlation approach becomes obvious, because due to its

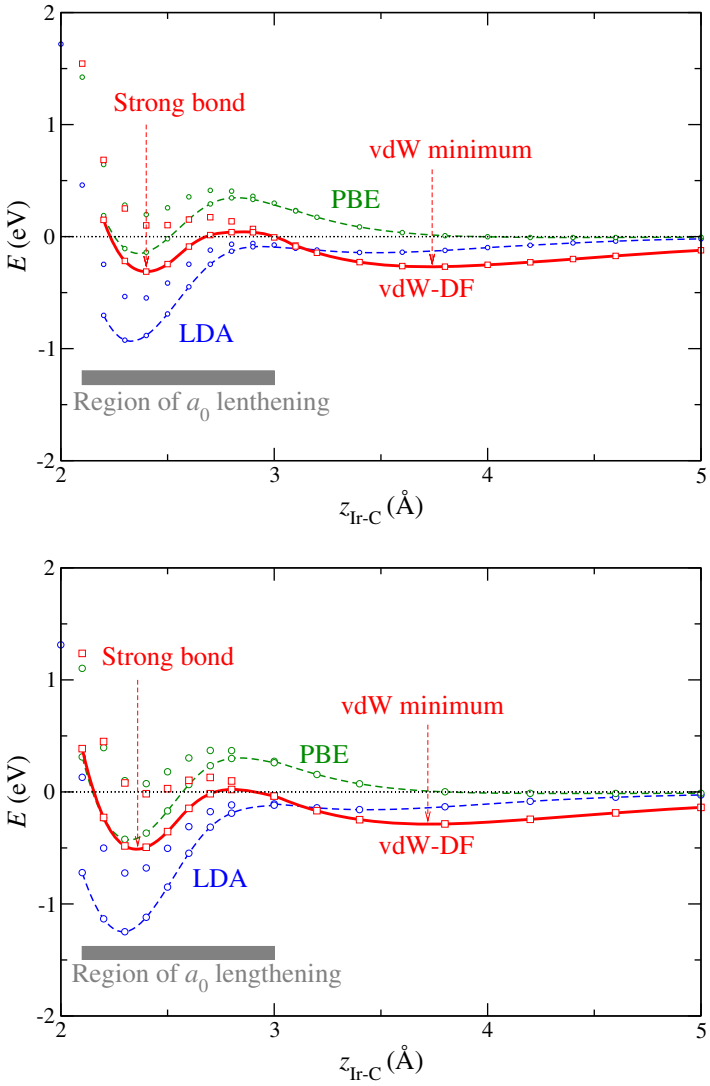

Figure 7. Standard DFT (LDA and PBE GGA) and vdW-DF energies for Ir–graphene–Ir sandwiches, structures (c) and (d) in figure 4. The lines connect points for which the energy has the minimum when allowing the structures to slightly expand laterally, as explained in the text.

'seamless' character we can apply it at all graphene–Ir distances, i.e. at all coupling strengths, without worrying that it may spoil the GGA results, which are good for strong bonding.[7]

The results for structure (a) are shown by squares in figure 6, where the PBE and the LDA results are the same as in figure 5, and the energy calculated using vdW-DF is shown by a thick line and squares. A clear vdW attractive well develops, deeper than the shallow well in the LDA calculation and with the minimum at a larger graphene–substrate distance, about 3.7 Å. Figure 7 shows similar results for structures (c) and (d). The unconnected points are for the lattice constant of free graphene, as in figure 5, and the points connected by lines are

[7] In fact, in some cases the nonlocal correlation makes crucial improvements to the description of strongly bound systems, as has been recently shown for the known 'puzzle' of CO chemisorbed on transition metal surfaces [23].

Table 1. Bond length and angles of structure (a) at energy minimum and of structures (c) and (d) at the strong bonding energy minima. All lengths are in Å. Here a_0 is the optimal lattice constant of the structure in the x–y plane, which for (c) and (d) is slightly larger than the free graphene value of 3.478 Å, z_{S-A} is the distance between the substrate atom Ir_S and C_A, z_{buck} is the buckling of graphene, i.e. the difference of the z-coordinates of atoms C_A and C_B, z_{B-O} the distance between C_B and the overlayer atom Ir_O, d_{A-B} the distance between two neighbouring C atoms and α the angle defined by the lines Ir_S–C_A and C_A–C_B.

Structure	a_0	z_{S-A}	z_{buck}	z_{B-O}	d_{A-B}	α
(a)	3.478	3.7	0	—	1.42	90°
(c)	3.65	2.17	0.40	2.17	1.54	105°
(d)	3.72	2.22	0.41	2.17	1.57	105.3°

for the optimized expanded lattice constant. The vdW potential well is similar to figure 6 but is approximately twice as deep (note the different scale on the energy axis), since the graphene interacts with both the iridium substrate and overlayer. The depth and shape of the chemisorption minimum at about 2.3 Å is less affected by the non-local correlation, but the barrier between the two minima is much decreased compared with the PBE results.

4.3. Discussion of the results

Detailed information about the nature of C–C and C–Ir bonds can be inferred by examining the geometry of the graphene lattice around the minima of the interaction energy in figure 7. At the physisorption minimum, $z_{Ir-g} \sim 3.7$ Å, the graphene lattice is perfectly planar, and the graphene stays at the midpoint between two neighbouring iridium layers. The same is true for all structures in figure 4 and in fact for other geometries such as monolayer graphene over the 1–2 and 2–3 regions in figure 3. Due to the smoothness of the potential with respect to the translation of graphene along the surface, graphene flakes physisorbed on Ir(111) are quite mobile, both translationally and rotationally, which is an important mechanism in the aggregation and growth of large graphene islands [24].

The situation is rather different when strong bonding between iridium and graphene in Ir–graphene–Ir structures occurs, at $z_{Ir\text{-}g}$ around 2.3 Å in figure 7. First, we note that the total energy depends strongly on the position of the C atoms of graphene with respect to the Ir atoms below and above. Thus, the two similar structures, (b) and (d) in figure 4, differ only in the position of the iridium atoms in the monoatomic overlayer, but the total energies in figure 5 differ by more than 1 eV! The absence of a stable strong bond in structure (b) shows that strong bonding can occur only when both C atoms are saturated by Ir atoms, one directly below or above each. This immediately implies that the onset of strong bonding effectively anchors the iridium cluster and the underlying graphene to a particular spot of the moiré pattern of the graphene–substrate supercell.

The formation of the strong 'organometallic' bond is accompanied by the buckling of graphene and C–C bond lengthening. Table 1 shows the values of bond lengths and angles corresponding to the strong bonding energy minima in the two panels of figure 7. These

values are close to the those of tetrahedrally bonded C atoms in diamond, and indicate that rehybridization from sp^2 to sp^3 bonding has occurred, as noted by Feibelman [9].

5. Discussion

These results show that the onset of the strong C–Ir binding in Ir–graphene–Ir sandwiches is accompanied by the disappearance of the aromatic character of the carbon rings. The carbon atoms rehybridize to sp^3 configuration, and the two C atoms in the graphene unit cell move out of the plane in opposite directions. On the other hand, in one-sided binding on Ir(111) (i.e. a clean graphene overlayer) the C–Ir bond is always weak, dominated by vdW interaction.

The strength of binding of adsorbed graphene is, of course, strongly correlated with its electronic band structure. As already mentioned, the weak binding of graphene monolayer on Ir(111) leaves the electronic π-bands of graphene largely intact, and Dirac cones have been clearly observed in angularly resolved photoemission experiments [22]. The situation is quite different in the cases of strong binding. Thus, the π-bands of graphene on Ni(111) are strongly modified and a large band gap opens, but upon the intercalation with one monolayer of Au the bonding reverses to weak, the gap closes and the graphene π-bands show linear dispersion with the Dirac point exactly at the Fermi energy [25].

A transition to strong bonding of graphene on Ir(111) has also been observed upon the adsorption of atomic hydrogen on graphene [26]. STM images show that the adsorption is patterned, occurring only in bright parts of the moiré superstructure. Photoemission measurements reveal that this is accompanied by the opening of a gap of at least 450 meV in the dispersion of the π-band. In order to interpret these findings, DFT calculations of various hydrogen adsorbate structures on graphene have been performed. They show that it is energetically favourable for adsorbed hydrogen to arrange in 'graphane-like' islands, where every other C atom binds to a hydrogen atom above and every other to an Ir atom below, resulting in a local rehybridization from sp^2 to sp^3 bonding. This is completely analogous to the structure of the most stable Ir–graphene–Ir sandwich structure in the present paper. In the case of Ir clusters on top of graphene on Ir(111), there are no photoemission measurements of the graphene electronic bands yet, but the strength of the bonding indicates that a significant change of the π-bands with a gap opening at the Dirac points should be expected.

In order to gain more insight into the character of the bonding of aromatic rings on Ir(111), we have made DFT calculations of benzene molecules C_6H_6 lying flat on the iridium surface. We found large differences in binding energies and distances for different positions of the benzene molecules with respect to the substrate atoms. The most stable configuration is when the centre of the ring is above a hollow site, and the six C atoms are above three Ir atoms, two C on each Ir. (This configuration cannot be directly compared to any part of the moiré pattern of graphene on Ir(111), figure 3, since it corresponds to a different orientation of the aromatic rings, i.e. rotated by 30°.) The C–Ir bond is around 2.4 Å. The GGA adsorption energy is somewhat less than 1 eV, and does not change substantially when the vdW-DF nonlocal correlation is used. The C atoms remain planar due to symmetry, but the C–C bonds become longer, 1.43 and 1.48 Å, and the H atoms are slightly above the plane of the C atoms. This indicates a change of the nature of the bonding of the carbon ring and a departure from the pure sp^2 hybridization. The other configurations, where the centre of the benzene ring is above an Ir atom and H atoms point either towards the neighbouring Ir atoms or towards bridge sites, are more weakly bound. The C–Ir bond length is around 3.4 Å. In this case, the non-local correlation is essential for the bonding.

With pure GGA functional there is virtually no bonding of the benzene molecule, while with the vdW-DF the bonding energy is around 0.6 eV. The C–C bonds keep the value of 1.41 Å as in the benzene molecule, and the whole benzene structure is planar. These values are also very similar to those of graphene on Ir(111) obtained earlier, indicating a weak, vdW-dominated bonding. Thus, the bonding of benzene on Ir(111) shows even more variation of bonding parameters than various regions of the moiré of graphene, showing the richness of possible bonding of aromatic structures (molecules and graphene) on metal surfaces.

Graphene strongly binds on some other surfaces, as mentioned in the introduction, apparently without strong rehybridization to sp^3. In a recent combined experimental and theoretical study of graphene bonding on the Ru(0001) surface [7], it was found that graphene is strongly corrugated with a minimum C–Ru distance of 2.1 Å and a corrugation of 1.53 Å in the regions of strong coupling. DFT calculations were performed using the standard PBE functional, which is expected to work well in regions of strong coupling, and the lack of vdW interaction that should be dominant in the weakly coupled 'blisters' is not crucial. The authors found that the height difference between neighbouring C atoms in the graphene layer is below 0.03 Å in the strong coupling region in DFT, and concluded that the adsorbed graphene layer remains sp^2 hybridized.

Returning to the calculations of graphene on Ir(111), we note that the use of the large supercell in [9] has the advantage that the lattice constants of both the iridium substrate and the graphene overlayer can be kept close to their natural values. Thus, the problems that we encountered with our compressed Ir surface (expanded in the z-direction) are avoided. In particular, it seems that we get somewhat too large Ir–graphene distances compared to other calculations and the preliminary experimental estimates. Furthermore, when iridium clusters are added on top of graphene, in the large supercell approach the carbon atoms are free to relax both vertically and laterally, which is essential for a good description of graphene buckling and the formation of a strong C–Ir bond. In section 4.2, we had to use a calculation tour de force to detect the preference of carbon atoms to lengthen somewhat the C–C bonds and thus approach more closely the diamond structure. Furthermore, in the supercell approach the substrate iridium atoms may also relax laterally, optimizing the saturation of the bonds to carbon atoms.

These advantages come with the downside that in [9] the LDA functional was used. This was a necessary choice since GGA in the usual formulation, i.e. without the vdW interaction being somehow accounted for, gives little or no binding of graphene (see [8], in particular the erratum). However, LDA usually gives too small an equilibrium distance, and overbinds in cases of strong chemical bonding. Thus, in our calculations of graphite in section 2, figure 2, LDA gave too small an interlayer distance. Our LDA binding energy of graphite was also too small, since graphite is a system with very little chemical component of the bond and the LDA overbinding could not compensate fully for the absence of the vdW component.

The compressed Ir(111) surface in our approach and the use of LDA in [9] preclude a detailed quantitative comparison between the results of the two calculations, and of each of them with experiment. However, the semiquantitative agreement is good. Both approaches predict a rather weak bonding of a graphene monolayer with the Ir(111) substrate, and the formation of a much stronger organometallic bond when iridium clusters are added on top, accompanied by the buckling of the graphene structure and shortening of Ir–C distances. For clean graphene, the Ir–C separation at the 1–3 regions of the moiré pattern is about 3.48 Å in [9] and about 3.7 Å in our work. When the clusters trigger strong bonding and graphene buckling the Ir–C distance

decreases to about 2.1 Å in [9] and to about 2.2 Å in our work, while the Ir–C–C angles are about 105°.

The bonding of graphene to some other (111) surfaces of fcc metals assuming commensurate configurations has also been investigated. In the papers by Giovannetti *et al* [19] and Khomyakov *et al* [27], the LDA functional was used. The unit cells were either two graphene C atoms and one metal atom in each layer (e.g. Ni, Co and Cu), as in our calculation, or eight C atoms and three metal atoms with the graphene unit cell rotated by 30° when the difference of the lattice constants was larger (e.g. Pd, Au and Pt). It was found that graphene interacts strongly with Ni, Co and Pd, with the equilibrium metal–graphene distance between 2.05 and 2.30 Å, and weakly with Cu, Au and Pt, with equilibrium distance between 3.26 and 3.31 Å. These findings are in agreement with experiment, where available. The mismatch of the lattice constant of graphene is 4% for Cu, 1.2% for Ni and 2% for Co (the metal unit cell being larger in all three cases). This is clearly smaller than in our calculation, where the difference of Ir(111) and graphene lattice constants is about 10%.

Vanin *et al* [20] consider the same surfaces, but in a different approach. They use the vdW-DF correlation functional [12] evaluated using the method proposed in [28] and self-consistently implemented into the real-space projector augmented wave gpaw code [11]. They do not adjust the metal substrate to match the lattice constant of graphene as we do, but instead keep it at their experimental lattice parameters and adjust the graphene sheet. They claim that the vdW-DF results do not change significantly if they fix the graphene lattice parameter to its optimized value and adjust the metals correspondingly. They obtain weak binding for all metals considered, with metal–graphene distances in the range of 3.40–3.72 Å. This is in clear disagreement with the case of Ni(111), where strong binding has been experimentally confirmed. This result is somewhat surprising, since the match between the lattice constants of graphene and Ni(111) is almost perfect, and no artificial lattice adjustment is necessary.

The graphene is particularly stable due to the aromatic character of the carbon rings. Perturbing the structure (for example by forcibly changing the natural bond length) may significantly change the reactivity. Thus, simply adapting the graphene lattice constant to the substrate may have unwanted consequences, weakening the stability of the aromatic bonds, as well as changing the doping of the graphene layer in contact with the metal surface. The opposite procedure, which we used in this paper, i.e. adapting the substrate lattice constant, seems preferable to us, although it may also have some weaknesses. First, the change of the electronic structure of the substrate may be large enough to alter the reactivity compared to the natural metal. Also, the lattice constant of the free graphene may not be optimal for rehybridized graphene forming strong sp^3 bonds. We had to expand the graphene lattice slightly in order to obtain a sufficiently stable strong bonding. In the process we had to carefully account for the change in energy of the iridium substrate, which was, of course, also expanded (i.e. less compressed compared to the natural structure). All this indicates that the graphene lattice constant should be left at its natural value in the weak bonding cases, but should be allowed to relax and lengthen when the strong bonding regime accompanied by graphene buckling and rehybridization to diamond-like bond occurs. This cannot be achieved in the simplified commensurable geometries, and a full large supercell calculation with state-of-the-art non-local correlation functional seems to be the only approach that can give a clue to the structure of graphene adsorbed on various metals in the general case. We expect that the progress in the implementation of the non-local functionals and of the computing power will soon make such large supercell calculations possible.

6. Conclusions

We find that a graphene monolayer on Ir(111) is weakly bound, and keeps the aromatic character of the carbon rings. In Ir–graphene–Ir structures C atoms show a tendency towards rehybridization and formation of sp^3 bonds, which in favourable cases (an Ir atom directly below or above each C atom) are more stable than the physisorbed structure. We conclude that this system is on the verge of weak vdW and strong 'organometallic' binding which both have to be correctly described. Theoretical considerations indicate that non-local correlation is essential for a proper description of the system. Our calculations show that DFT with the non-local functional vdW-DF can reproduce the observed behaviour. Our approach in which the substrate lattice constant is adjusted to match graphene does not give full quantitative accuracy. To obtain that kind of agreement, large calculations on realistic supercells using DFT functionals with non-local correlation are necessary. This conclusion is also true for other graphene-on-metal systems, in which the nature of the graphene–metal bond may be different from that on Ir(111).

Acknowledgments

This work was supported by the Ministry of Science, Education and Sports of the Republic of Croatia, under contract no. 098-0352828-2863. P Lazić acknowledges financial support from the Alexander von Humboldt Foundation. The calculations were performed on JUROPA and JUGENE supercomputers at the Jülich Supercomputing Centre, Forschungszentrum Jülich, Germany.

References

[1] Geim A K and Novoselov K S 2007 The rise of graphene *Nat. Mater.* **6** 183
[2] Lee C, Wei X, Kysar J W and Hone J 2008 Measurement of the elastic properties and intrinsic strength of monolayer graphene *Science* **321** 385
[3] Wintterlin J and Bocquet M-L 2009 Graphene on metal surfaces *Surface Sci.* **603** 1841
[4] Bertoni G, Calmels L, Altibelli A and Serin V 2004 First-principles calculation of the electronic structure and EELS spectra at the graphene/Ni(111) interface *Phys. Rev.* B **71** 075402
Fuentes-Cabrera M, Baskes M I, Melechko A V and Simpson M L 2008 Bridge structure for the graphene/Ni(111) system: a first principles study *Phys. Rev.* B **77** 035405
[5] Marchini S, Günther S and Wintterlin J 2007 Scanning tunneling microscopy of graphene on Ru(0001) *Phys. Rev.* B **76** 075429
[6] Martoccia D *et al* 2008 Graphene on Ru(0001): a 25 × 25 supercell *Phys. Rev. Lett.* **101** 126102
[7] Moritz W, Wang B, Bocquet M-L, Brugger T, Greber T, Wintterlin J and Günther S 2010 Structure determination of the coincidence phase of graphene on Ru(0001) *Phys. Rev. Lett.* **104** 136102
[8] N'Diaye A T, Bleikamp S, Feibelman P J and Michely T 2006 Two-dimensional Ir cluster lattice on a graphene moiré on Ir(111) *Phys. Rev. Lett.* **97** 215501
N'Diaye A T, Bleikamp S, Feibelman P J and Michely T 2008 *Phys. Rev. Lett.* **101** 219904 (erratum)
[9] Feibelman P J 2008 Pinning of graphene to Ir(111) by flat Ir dots *Phys. Rev.* B **77** 165419
[10] Gonze X *et al* 2002 First-principles computation of material properties: the ABINIT software project *Comput. Mater. Sci.* **25** 478
[11] Mortensen J J, Hansen L B and Jacobsen K W 2005 Real-space grid implementation of the projector augmented wave method *Phys. Rev.* B **71** 035109

[12] Dion M, Rydberg H, Schröder E, Langreth D C and Lundqvist B I 2004 Van der Waals density functional for general geometries *Phys. Rev. Lett.* **92** 246401
Dion M, Rydberg H, Schröder E, Langreth D C and Lundqvist B I 2005 *Phys. Rev. Lett.* **95** 109902 (erratam)
[13] Lazić P, Atodiresei N, Alaei M, Caciuc V, Blügel S and Brako R 2010 JuNoLo – Jülich nonlocal code for parallel post-processing evaluation of vdW-DF correlation energy *Comput. Phys. Commun.* **181** 371
[14] Langreth D C *et al* 2009 A density functional for sparse matter *J. Phys.: Condens. Matter* **21** 084203
[15] Thonhauser T, Cooper V R, Li S, Puzder A, Hyldgaard P and Langreth D C 2007 Van der Waals density functional: self-consistent potential and the nature of the van der Waals bond *Phys. Rev.* B **76** 125112
[16] Spanu L, Sorella S and Galli G 2009 Nature and strength of interlayer binding in graphite *Phys. Rev. Lett.* **103** 196401
[17] Dobson J F, White A and Rubio A 2006 Asymptotics of the dispersion interaction: analytic benchmarks for van der Waals energy functionals *Phys. Rev. Lett.* **96** 073201
[18] Lacovig P, Pozzo M, Alfè D, Vilmercati P, Baraldi A and Lizzit S 2009 Growth of dome-shaped carbon nanoislands on Ir(111): the intermediate between carbidic clusters and quasi-free-standing graphene *Phys. Rev. Lett.* **103** 166101
[19] Giovannetti G, Khomyakov P A, Brocks G, Karpan V M, van den Brink J and Kelly P J 2008 Doping graphene with metal contacts *Phys. Rev. Lett.* **101** 026803
[20] Vanin M, Mortensen J J, Kelkkanen A K, Garcia-Lastra J M, Thygesen K S and Jacobsen K W 2010 Graphene on metals: a van der Waals density functional study *Phys. Rev.* B **81** 081408
[21] Pletikosić I, Kralj M, Šokčević D, Brako R, Lazić P and Pervan P 2010 Photoemission and density functional theory study of Ir(111); energy band gap mapping *J. Phys.: Condens. Matter* **22** 135006
[22] Pletikosić I, Kralj M, Pervan P, Brako R, Coraux J, N'Diaye A T, Busse C and Michely T 2009 Dirac cones and minigaps for graphene on Ir(111) *Phys. Rev. Lett.* **102** 056808
[23] Lazić P, Alaei M, Atodiresei N, Caciuc V, Brako R and Blügel S 2010 Density functional theory with nonlocal correlation: a key to the solution of the CO adsorption puzzle *Phys. Rev.* B **81** 045401
[24] Coraux J, N'Diaye A T, Engler M, Busse C, Wall D, Buckanie N, Meyer zu Heringdorf F-J, van Gastel R, Poelsema B and Michely T 2009 Growth of graphene on Ir(111) *New J. Phys.* **11** 023006
[25] Varykhalov A, Sánchez-Barriga J, Shikin A M, Biswas C, Vescovo E, Rybkin A, Marchenko D and Rader O 2008 Electronic and magnetic properties of quasifreestanding graphene on Ni *Phys. Rev. Lett.* **101** 157601
[26] Balog B *et al* 2010 Bandgap opening in graphene induced by patterned hydrogen adsorption *Nat. Mater.* **9** 319
[27] Khomyakov P A, Giovannetti G, Rusu P C, Brocks G, van den Brink J and Kelly P J 2009 First-principles study of the interaction and charge transfer between graphene and metals *Phys. Rev.* B **79** 195425
[28] Román-Pérez G and Soler J M 2009 Efficient implementation of a van der Waals density functional: application to double-wall carbon nanotubes *Phys. Rev. Lett.* **103** 096102